Quality Criteria Benchmark for Hyperspectral Imagery

Emmanuel Christophe, *Student Member, IEEE*, Dominique Léger, and Corinne Mailhes, *Member, IEEE*

***Abstract*—Hyperspectral data appear to be of a growing interest over the past few years. However, applications for hyperspectral data are still in their infancy as handling the significant size of the data presents a challenge for the user community. Efficient compression techniques are required, and lossy compression, specifically, will have a role to play, provided its impact on remote sensing applications remains insignificant. To assess the data quality, suitable distortion measures relevant to end-user applications are required. Quality criteria are also of a major interest for the conception and development of new sensors to define their requirements and specifications. This paper proposes a method to evaluate quality criteria in the context of hyperspectral images. The purpose is to provide quality criteria relevant to the impact of degradations on several classification applications. Different quality criteria are considered. Some are traditionnally used in image and video coding and are adapted here to hyperspectral images. Others are specific to hyperspectral data. We also propose the adaptation of two advanced criteria in the presence of different simulated degradations on AVIRIS hyperspectral images. Finally, five criteria are selected to give an accurate representation of the nature and the level of the degradation affecting hyperspectral data.**

***Index Terms*—Classification, compression, evaluation, hyperspectral, quality criteria.**

I. Introduction

REMOTE sensing applications have been of a growing interest since a few decades ago. As these applications seek better quality data, performances of sensors improve with an increase in the spatial resolution, the radiometric precision, and possibly the number of spectral bands. This holds for hyperspectral imagery as well. Hyperspectral imagery, or spectral imagery, consists in observing the same scene at different wavelengths. Typically, every pixel of the image is represented by hundreds of values, each corresponding to a different wavelength. These values correspond to a sampling of the continuous spectrum emitted by the pixel. This high-resolution spectral sampling allows pixel identification: materials, type of vegetation, etc. The availability of the spectral information for each pixel leads to new applications in all fields that use remote sensing data such as agriculture, environment, or military.

Manuscript received November 19, 2004; revised April 6, 2005. This work was carried out under the financial support of Centre National d'Études Spatiales (CNES), Office National d'Études et de Recherches Aérospatiales (ONERA), and Alcatel Space.

E. Christophe and C. Mailhes are with the Institut de Recherche en Informatique de Toulouse, TéSA, 31000 Toulouse, France (e-mail: e.christophe@ieee.org; corinne.mailhes@enseeiht.fr).

D. Léger is with the Optics Department, Office National d'Études et de Recherches Aérospatiales, 31055 Toulouse, France (e-mail: dominique.leger@onera.fr).

Digital Object Identifier 10.1109/TGRS.2005.853931

These factors caused a rapid development of airborne and spaceborne hyperspectral imagery resulting in a phenomenal increase in the amount of available information. While this is useful for remote sensing applications, it produces images of a considerable size. Currently, the amount of information transmitted is limited by the available bandwidth and by the onboard storage capacity. Therefore, the compression step becomes a crucial part of the acquisition system to enhance the ability to store, access and transmit information.

Onboard compression in space probes or satellites can enable time-continuous acquisitions. Ideally, the compression should be lossless to guarantee the best quality of information. However, lossless compression techniques such as DPCM, do not give compression ratios higher than two or three [1]. This limitation is due mainly to the noise of high-resolution sensors [2]. Consequently, research is currently oriented toward near-lossless compression.

Since compression algorithms have to be implemented onboard, i.e., before the space to ground transmission, information losses due to compression will be irrecoverable. One may find the loss of information difficult to accept, but this loss would enable sensors to acquire and transmit more images at a faster rate. Furthermore, suppressing the less important information makes it possible to acquire more useful information. A few years ago, compression losses seemed unacceptable for scientific applications. Now, end-users are more willing to accept lossy compression as its advantages are better understood. However, when dealing with lossy data compression, it is important to define quality criteria, or distortion measures, that are able to quantify properly the information loss due to compression algorithms. These criteria can be used to ensure that no critical information has been lost during the compression process, and that the scientific value of the original data is preserved.

Specifications of future hyperspectral instruments need quality criteria to be more accurate. Usually, during the definition process, extensive simulations are conducted to assess the performances of the new system. For example in classical imagery, the modulation transfer function (MTF) is used extensively during sensors specifications.

For these reasons, the need for quality criteria becomes apparent. Quality criteria should be easily applicable to measure the loss of information caused by compression or by some other forms of processing. In the case of ordinary two-dimensional (2-D) images, the quality criterion has to reflect the visual perception of a human observer. Indeed, in most cases, the human is at the end of the imaging chain. This is not the case for hyperspectral images, therefore, quality criteria have to be relevant to the corresponding applications. For example, some papers

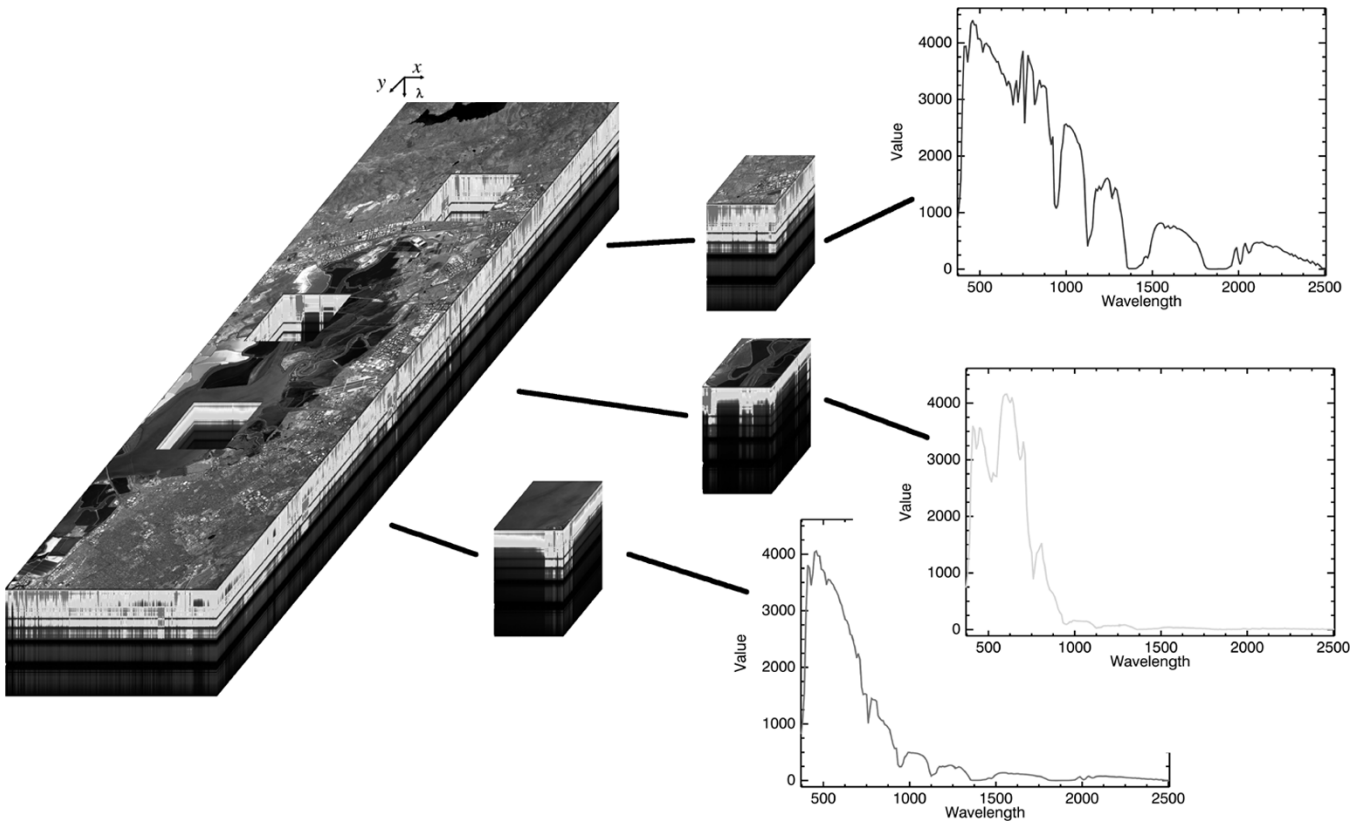

Fig. 1. Hyperspectral data (Moffett Fields by AVIRIS in 1997). The top of the cube is a color composite (shown in grayscale) of three spectral bands. The sides of the cube display the spectra of the pixels. The spectral dimension is represented vertically. On the middle, three hyperspectral cubes from three different areas are extracted. On the right, mean spectra for the three extracted cubes are presented. Spectral signatures provided by hyperspectral images can be used to identify specific materials.

[3]–[5] address the problem of evaluating compression impact on specific hyperspectral applications.

The goal of this paper is to define a panel of quality criteria that can be relevant to different classification methods in hyperspectral imagery. Section II introduces hyperspectral images, their applications, and their typical degradations. Section III elaborates on quality criteria and proposes some specific ones. Section IV defines a process of evaluation to compare performances of different quality criteria according to their abilities to reflect the loss in classification performances. Finally, Section V gives comparison results and proposes a set of quality criteria adapted to hyperspectral imagery. Perspectives are reported in the last section.

II. Hyperspectral Data

A. Hyperspectral Specificities

A hyperspectral image is acquired by imaging spectrometers [6]. The same scene is observed at different wavelengths. The main differences between multispectral and hyperspectral imagery are in the number of bands (usually 100–200 bands for hyperspectral), the spectral width of these bands (narrow bands about 10–20 nm), and the fact that the bands are contiguous (Table I). The process of data acquisition is also different. In multispectral sensors, the separation between the different bands is generally done using filters or distinct acquisition systems whereas in the hyperspectral case, the light is sent through a dispersive element (a grating in most cases) to separate the different wavelength components. The light coming from one ground pixel is projected on a charge-coupled device (CCD) line. Each element of the line simultaneously receives a narrow wavelength band that corresponds to this ground pixel. This is the main reason why spectral bands of hyperspectral images are intrinsically contiguous. This acquisition process can be interpreted as a sampling of the spectrum of each pixel. The sampling interval has to be narrow enough to allow a good spectrum reconstruction.

TABLE I
Typical Spaceborne Hyperspectral Specifications (2004)

Spectral range	400-2500 nm
Spatial resolution	20 m
Bands	200
Spectral resolution	10 nm
Quantization	12 bits
Swath	20 km

The structure of hyperspectral images is not easy to analyze for nonspecialists of the domain. Thus, several ways of presenting these images can be used. First, hyperspectral data can be viewed as three-dimensional (3-D) data, with two spatial dimensions (image) and one spectral dimension (spectrum). Hyperspectral images are therefore often represented as cubes or *hypercubes* (Fig. 1).

However, viewing hyperspectral data as cubes is incomplete and neglects one important specificity of these images. This 3-D

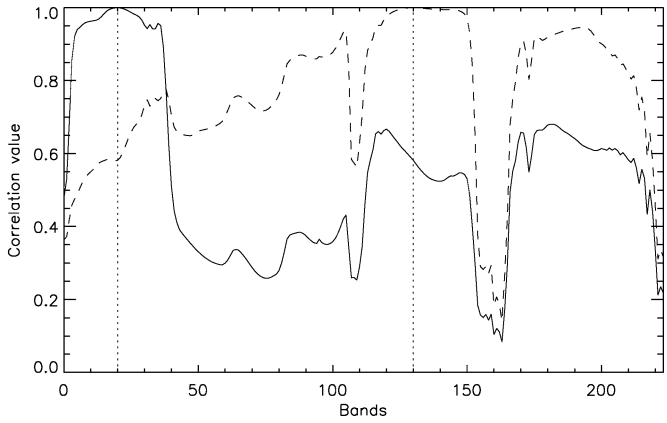

Fig. 2. Spectral correlation coefficient. Correlation between (solid line) band 20 and the other bands (respectively, band 130 (dashed) and the other bands). The correlation can remain significant even if the distance between bands increases, e.g., correlation coefficient between bands 20 and 180 is greater than 0.6.

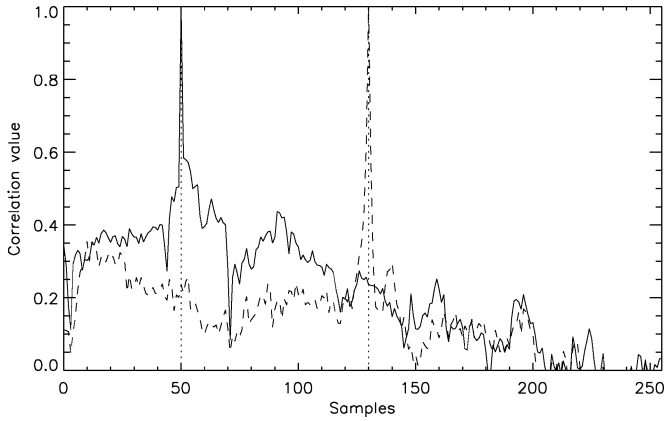

Fig. 3. Spatial correlation coefficient. Correlation between (solid line) sample 50 and other samples (respectively, sample 130 (dashed) and the other samples). The correlation between samples drops sharply as the distance increases: with a distance greater than ten samples, the correlation coefficient is below 0.4.

view considers all the three dimensions as equivalent, which is not the way they should be analyzed. Indeed, these three dimensions possess different characteristics. Their statistical properties are not the same. For example, the correlation that appears in the spectral dimension between two distant bands (Fig. 2) is completely different from the short-range correlation in spatial dimensions (Fig. 3). Due to these differences, the hypercube is nonisotropic and there are more suitable ways to interpret hyperspectral data.

The first nonisotropic way, also the most intuitive, is to see hyperspectral data as a stack of images for different wavelengths. This view comes directly from multispectral image interpretation. When considering hyperspectral data this way, typical image processing algorithms can be used. Each classical 2-D image is processed, independently from the others. Results from the different wavelengths are consolidated and merged.

The second way of considering hyperspectral images is to focus mainly on the spectral dimension. Each pixel of a hyperspectral image can be seen as a vector on an n_λ-dimensional basis (with n_λ be the number of spectral bands). When considering the data this way, applications from signal processing can be used. This spectral representation leads to typical hyperspectral applications based on spectral identification. It has to be emphasized that when considering an n_λ-dimensional basis, some unusual problems occur, known collectively as *curse of dimensionality* [7]. To avoid these problems, pretreatments, such as principal component analysis, are often used to reduce the number of dimensions [6].

Another specificity of hyperspectral data becomes apparent when considering the data size. With 242 spectral samples for each pixel, a radiometric resolution of 12 bits, and a scene of 256×660 pixels (NASA/TRW spaceborne imager Hyperion on the Earth Observing 1), the size of one image can easily reach 490 Mb for an area of 7.5 $\times$ 19.8 km (about 3 s of data acquisition) [8]. The data rate available for current hyperspectral spaceborne sensors is currently 105 Mb/s, and the trend is to increase the spatial and spectral resolutions. The airborne imager AVIRIS (NASA/JPL) has equivalent characteristics in term of amount of data.

B. Applications of Hyperspectral Data

Hyperspectral images are used in various fields from agriculture (ground use monitoring) to military (detection, recognition, and identification) and from environment (ocean or forestry monitoring) to geology (mineral, oil, gas exploration). Thus, hyperspectral imagery applications can include several objectives: target detection, material mapping, material identification or mapping details of surface properties. Indeed, the availability of a spectral signature for each pixel provides the potential for more accurate and detailed information extraction than is possible with multispectral or other types of imagery.

This particular use of hyperspectral data, i.e., focusing more on the spectral information than on the spatial contents, creates a significant difference with the approach of traditional imagery: the spectral information (used for spectral identification) has to be preserved.

The second specific point about hyperspectral applications comes from the significant amount of data involved. While traditional remote sensing images generally have photointerpreters as viewers, leading to the development of quality criteria based on the human visual system (HVS), hyperspectral data are processed by a wide range of automated algorithms. This particular feature makes the quality criteria developed for the HVS irrelevant.

C. Typical Degradations From the Acquisition Process

As remote sensing data, hyperspectral images suffer from degradations due to the acquisition process. Different degradations are introduced by the acquisition system in the image, causing a loss of image quality.

The first degradation on the data is radiometric noise caused mainly by photonic effects in the photon detection process, by electronic devices, and by quantization. This noise can often be assimilated to white noise even if some correlation exists between different bands [9]. Noise is often measured by the signal-to-noise ratio (SNR) value. Typically, the SNR value is over 500 : 1 on most of the spectral range for AVIRIS (1995 instrument version [10], corresponding to images of Moffett

Fields dated 1997) or 150 : 1 for Hyperion (in visible and near-infrared [11]).

Other degradations are due to the optical characteristics of the spectroimagers. The point spread fnction (PSF) can cause a smoothing effect along the spatial dimension [11]. The dispersion element and the CCD characteristics can produce a smoothing effect along the spectral dimension. Some posttreatments, including filtering, compression, or decorrelation, can also produce some smoothing effects as well as Gibbs effect (ringing around sharp changes).

Like multispectral sensors, hyperspectral data can be affected by registration problems. Misregistration corresponds to a bad alignment between spectral bands. However, due to the acquisition process, this effect is much more limited for hyperspectral data compared to multispectral data. While it can be of a few pixels for multispectral, it is lower than 0.2 pixels for hyperspectral [12]. Other effects such as *smile* or *keystone* can appear due to instrument conception defaults. However, current designs for hyperspectral instruments can virtually eliminate these classical problems [13]. Therefore, this kind of degradation will not be considered in this paper.

During the characterization of an instrument, quality criteria related to application needs will help to enhance its performance by highlighting the crucial characteristics to improve. Reducing the instrument noise is a key feature for data quality improvement. Quality criteria representative of the end-user applications can help to focus on the critical characteristics to improve.

III. Quality Criteria for Hyperspectral

A. Quality Criteria in General

In many domains, there is a need for quality criteria. For example, in classical image processing, criteria such as mean square error (MSE) or SNR are used even though it is well known that standard metrics do not reflect the perceived information loss properly. To improve criteria for classical images, modeling for HVS has been developed.

In remote sensing field, quality criteria are used to characterize the requirements of an application from the imaging chain. The quality criteria should take into account all aspects of the data collection. Some criteria are strongly related to instrument characteristics, for example radiometric noise or modulation transfer function (MTF). Some other criteria are more specific and are difficult to define. This will be the case for say, a criterion representing the blocking effect of discrete cosine transform-based JPEG compression.

Image quality metrics can be divided into the follwing three categories [14]:

- *full reference metrics or bivariate:* measuring the quality between the original and the distorted image;
- *reduced reference metrics*: instead of using the whole original image, this method uses only a description of it that comprises of parameters (mean, variance, etc.);
- *no reference metrics:* using only the distorted image.

The full reference metrics are more accurate and more robust since all original information is available and can be compared with the distorted one. In the context of compression algorithm evaluation, full reference metrics are the ideal choice since the original image is available. For sensor definition, images are simulated and original images can be used as references. Therefore, in this paper, only full reference metrics will be considered.

The purpose of this evaluation is to find the *most suitable* quality criteria for hyperspectral imagery. Such evaluations have been done for ordinary still images [15] and are currently done for video sequences [16]. *Most suitable* means giving an accurate evaluation of the performances of traditional hyperspectral applications on images that are subjected to a set of degradations. A *good* criterion should react to the degradations that cause a loss in scientific value for the application; it should not react if the application is insensitive to a particular degradation.

One may wonder why quality criteria are used instead of evaluating degradations directly by the applications. There are several reasons. First of all, quality criteria tend to be more generic than applications. A quality criterion, or a set of criteria, can be representative of a large set of applications. The second reason resides in the fact that quality criteria are easy to apply. No additional information is needed to compute them while this is not the case for applications (classification applications require ground truth or defined regions of interest, detection applications require spectral characteristics, etc.). The third reason is that the computation time for quality criteria is just a few seconds while hyperspectral applications are more complex and require minutes or hours.

B. Adaptation to Hyperspectral Images

Many quality criteria have been defined in the literature: [3], [17]–[19], for example. For their adaptation to hyperspectral images, these criteria can be divided into three categories. The first one is composed of traditional criteria used in image or video processing. These criteria can be extended directly to the third dimension of hyperspectral images. In this case, the specificity of hyperspectral, explained in Section II-A, is not considered. The second group of criteria is more specific to hyperspectral since they really focus on considering spectral information. In most cases, these criteria are defined on spectral vectors. Finally, the last group contains different adaptations of two advanced criteria for ordinary images. We propose to adapt them for hyperspectral images taking into account the specificity of hyperspectral data.

As the quality measures included in the evaluation are bivariate, they provide a measurement of the distance between I, the original hyperspectral image, and $\widetilde{I}$, the degraded one. Images are also written in a matrix form, where $I(x, y, \lambda)$ denotes the value from the column x of row y in the spectral band λ. Values n_x, n_y and n_λ are the numbers of, respectively, columns, rows, and spectral bands. To simplify, we will denote $\sum_{x=1}^{n_x}\sum_{y=1}^{n_y}\sum_{\lambda=1}^{n_\lambda} I(x, y, \lambda)$ as $\sum_{x,y,\lambda} I(x, y, \lambda)$ and $e_{\widetilde{I}}(x, y, \lambda) = I(x, y, \lambda) - \widetilde{I}(x, y, \lambda)$.

The standard $\mathcal{L}_p$ norm is defined as

$$\mathcal{L}_p(I) = \|I\|_p = \left(\sum_{x,y,\lambda} |I(x, y, \lambda)|^p\right)^{\frac{1}{p}}. \quad (1)$$

The first five criteria, extended directly from widespread criteria, are as follows:

- mean square error

$$\mathrm{MSE} = \frac{\mathcal{L}_2^2(I - \widetilde{I})}{n_x n_y n_\lambda} \tag{2}$$

$$= \frac{1}{n_x n_y n_\lambda} \sum_{x,y,\lambda} \left(e_{\widetilde{I}}(x,y,\lambda) \right)^2. \tag{3}$$

Other formulations exist, such as root MSE, SNR, and peak SNR.

- relative RMSE (RRMSE)

$$\mathrm{RRMSE} = \sqrt{\frac{1}{n_x n_y n_\lambda} \sum_{x,y,\lambda} \left(\frac{e_{\widetilde{I}}(x,y,\lambda)}{I(x,y,\lambda)} \right)^2}. \tag{4}$$

- maximum absolute difference (MAD)

$$\mathrm{MAD} = \mathcal{L}_\infty(I - \widetilde{I}) = \max_{(x,y,\lambda)} \left\{ \left| e_{\widetilde{I}}(x,y,\lambda) \right| \right\}. \tag{5}$$

MAD can be used to bound the error within limits for any value of the original image. This property can be very useful in the case of local errors.

- percentage MAD

$$\mathrm{PMAD} = \max_{(x,y,\lambda)} \left\{ \frac{\left| e_{\widetilde{I}}(x,y,\lambda) \right|}{I(x,y,\lambda)} \right\} \times 100. \tag{6}$$

The main difference with MAD is in the tolerance of bigger errors for bigger values due to the introduction of the normalization term.

- mean absolute error (MAE)

$$\mathrm{MAE} = \frac{\mathcal{L}_1(I - \widetilde{I})}{n_x n_y n_\lambda} = \frac{1}{n_x n_y n_\lambda} \sum_{x,y,\lambda} \left| e_{\widetilde{I}}(x,y,\lambda) \right|. \tag{7}$$

The next four criteria, more specific to hyperspectral, are presented below. Let μ_U denote the mean of the set U and σ_U^2 its variance. The notation $I(x,y,\cdot)$ stands for $I(x,y,\cdot) = \{I(x,y,\lambda) | 1 \leqslant \lambda \leqslant n_\lambda\}$. In this case $I(x,y,\cdot)$ corresponds to a vector of n_λ components.

- maximum spectral similarity (MSS) [17]

$$\mathrm{MSS} = \max_{x,y} \left\{ \sqrt{\mathrm{RMSE}_{x,y}^2 + \left(1 - \mathrm{corr}_{x,y}^2\right)^2} \right\} \tag{8}$$

where

$$\mathrm{RMSE}_{x,y} = \sqrt{\frac{1}{n_\lambda} \sum_{\lambda} \left(e_{\widetilde{I}}(x,y,\lambda) \right)^2} \tag{9}$$

$$\mathrm{corr}_{x,y} = \frac{\sum_{\lambda} \left(I_c(x,y,\lambda) \right) \left(\widetilde{I}_c(x,y,\lambda) \right)}{(n_\lambda - 1) \sigma_{I(x,y,\cdot)} \sigma_{\widetilde{I}(x,y,\cdot)}} \tag{10}$$

with $I_c(x,y,\lambda) = I(x,y,\lambda) - \mu_{I(x,y,\cdot)}$ and $\widetilde{I}_c(x,y,\lambda) = \widetilde{I}(x,y,\lambda) - \mu_{\widetilde{I}(x,y,\cdot)}$.

The spectral similarity is defined as the combination of two separate measures of vector difference: a measure of spectral brightness and a measure of spectral shape.

- maximum spectral angle (MSA)

$$\mathrm{MSA} = \max_{x,y} \{ \mathrm{SA}_{x,y} \} \tag{11}$$

where

$$\mathrm{SA}_{x,y} = \cos^{-1} \left(\frac{\sum_{\lambda} I(x,y,\lambda) . \widetilde{I}(x,y,\lambda)}{\sqrt{\sum_{\lambda} I(x,y,\lambda)^2 \sum_{\lambda} \widetilde{I}(x,y,\lambda)^2}} \right). \tag{12}$$

The spectral angle represents the angle between two spectra viewed as vectors in an n_λ-dimensional space.

- maximum spectral information divergence (MSID) [18]

$$\mathrm{MSID} = \max_{x,y} \left\{ \sum_{\lambda} (p_\lambda - \tilde{p}_\lambda) \ln \left(\frac{p_\lambda}{\tilde{p}_\lambda} \right) \right\} \tag{13}$$

where $p_\lambda = I(x,y,\lambda) / \| I(x,y,\cdot) \|_1$ and $\tilde{p}_\lambda = \widetilde{I}(x,y,\lambda) \| \widetilde{I}(x,y,\cdot) \|_1$.

This criterion is based on the Kullback–Leibler distance, which measures the distance between two spectra viewed as distributions.

- minimum Pearson's correlation

$$\mathrm{Pearson} = \min_{x,y} \left\{ \mathrm{corr} \left(I(x,y,\cdot), \widetilde{I}(x,y,\cdot) \right) \right\}. \tag{14}$$

The criterion developed by Wang [20], Q, seems to give good results when applied to classical images. This criterion was also extended to video sequences. It is defined as

$$Q(U,V) = \frac{4 \sigma_{UV} \mu_U \mu_V}{(\sigma_U^2 + \sigma_V^2)(\mu_U^2 + \mu_V^2)} \tag{15}$$

where σ_{UV} is the covariance between U and V. This criterion can be written as a combination of three terms, measuring the correlation, the luminance distortion, and the contrast distortion.

From this definition, three hyperspectral specific formulations are proposed in the present paper. The first adaptation is spectrum oriented, while the second one corresponds to the view of hyperspectral data as a stack of images for different wavelengths. The last adaptation tries to combine properties of both.

- Q_λ

$$Q_\lambda = \min_{(x,y)} \left\{ Q \left(I(x,y,\cdot), \widetilde{I}(x,y,\cdot) \right) \right\}. \tag{16}$$

- $Q_{(x,y)}$

$$Q_{(x,y)} = \min_{\lambda} \left\{ Q \left(I(\cdot,\cdot,\lambda), \widetilde{I}(\cdot,\cdot,\lambda) \right) \right\}. \tag{17}$$

- Q_m

$$Q_m = Q_\lambda . Q_{(x,y)}. \tag{18}$$

Finally, we adapted the fidelity criterion defined by Eskicioglu [15], which gives good results when applied to grayscale images. Let the fidelity between two sets U and V be

$$F(U,V) = 1 - \frac{\mathcal{L}_2^2(U-V)}{\mathcal{L}_2^2(U)}. \quad (19)$$

Depending on the choice of U and V, we propose three adaptations. The first adaptation does not consider spatial and spectral dimension separately; this corresponds to the view of hyperspectral data as a hypercube. The second one is more spectrum oriented while the last one corresponds to the stack of images at different wavelengths.

- global fidelity

$$F = F(I,\widetilde{I}) = 1 - \frac{\sum_{x,y,\lambda}\left[I(x,y,\lambda) - \widetilde{I}(x,y,\lambda)\right]^2}{\sum_{x,y,\lambda}\left[I(x,y,\lambda)\right]^2}. \quad (20)$$

- spectral fidelity

$$F_\lambda = \min_{(x,y)}\left\{F\left(I(x,y,\cdot),\widetilde{I}(x,y,\cdot)\right)\right\}. \quad (21)$$

- spatial fidelity

$$F_{(x,y)} = \min_{\lambda}\left\{F\left(I(\cdot,\cdot,\lambda),\widetilde{I}(\cdot,\cdot,\lambda)\right)\right\}. \quad (22)$$

All these criteria are evaluated in Section IV. To sum up, among the 15 criteria we have the following.

- five are extended from statistical criteria: MSE, RRMSE, MAD, PMAD, and MAE;
- four are specific to hyperspectral: MSS, MSA, MSID, and Pearson;
- six are adaptations of image criteria: Q_λ, $Q_{(x,y)}$, Q_m, F, F_λ, and $F_{(x,y)}$.

This list is not exhaustive but the variety of the criteria evaluated seems sufficient to orientate further research.

IV. Evaluation Process

A. Quality Criteria for Image and Video Processing

The evaluation of quality criteria for hyperspectral imagery is similar to the validation of quality criteria for classical 2-D images or video sequences. When defining quality criteria for image or video processing, the objective is to reflect the human perception of the degradations. In the last 20 years, many papers have tried to define a method to benchmark different criteria [15], [21]. An adaptation from the *video quality expert group* (VQEG) [16] will be used here. The VQEG method is designed especially for video sequences with human users. Bivariate (full-reference) quality criteria are selected. These criteria are defined mathematically and they quantify degradations on video sequences objectively. On the other side, a panel of observers evaluates the image quality, giving a score (*mean opinion score*). This evaluation by observers is subjective and its variance may be significant. The purpose of the evaluation is to find the objective criteria that match the subjective evaluation best.

In the case of hyperspectral images, the main difference with traditional images and video is that human experts seldom process directly hyperspectral data. Most of the time, due to the sheer amount of information, data are directly processed by automated algorithms. For this reason, the *subjective* evaluation (according to the VQEG definition) does not correspond to a panel of observers, but to a panel of automated algorithms representing typical hyperspectral applications. We can expect all human observers to react in a similar way when subjected to the same degradation (within a certain variance). However such expectation may not be true for different hyperspectral applications. Applications may have a very different sensitivity to different degradations and we highlight this fact in Section V-A.

First, the images used during the evaluation process are presented and their main characteristics are highlighted. In the next paragraph, considered degradations are detailed, as well as their interpretation. Then, the reference applications used to benchmark quality criteria are reviewed. Finally, the evaluation process is defined.

B. Images

The SNR characteristics of the images chosen for the simulations are an important point to take into account. With a low SNR (high instrument noise), the added noise would be hidden under the instrument noise. Since the purpose of this study is to propose quality criteria for near-lossless compression, the impact of a very low level of noise has to be evaluated. Among all available hyperspectral images, images from AVIRIS NASA/JPL sensor present good SNR characteristics (about $500:1$) and will therefore be used in the following simulations. Airborne Visible Infrared Spectrometer (AVIRIS) data are available in radiance or reflectance. Degradations have been applied to radiance data in order to be as close as possible to real experimental conditions.

Simulations are done on two subsets of the Moffett Field site in California (AVIRIS run f970620t01p02_r03) with different properties. The part denoted *moffett2* (Fig. 4) contains large uniform zones (salt evaporator and sea) whereas *moffett3* (Fig. 5) is more uneven (man-made targets). *Moffett2* is the part of f970620t01p02_r03_sc03 from pixel (0,0) to pixel (255255) and *moffett3* from pixel (358256) to pixel (613511). The two subsets are 256×256 pixels with all the 224 bands.

C. Degradation Simulations

To provide accurate results, different degradations are applied to the selected hyperspectral images. Four different degradations at different levels are considered. These four types of degradation represent typical image degradations: Gaussian white additive noise, spatial or spectral smoothing, Gibbs effect, and lossy compression.

The first type of degradation applied to hyperspectral images is an additive Gaussian white noise with different variances. This noise models the instrumental photonic or electronic noise. A random noise of a given variance is added to the entire image.

A smoothing filter can be applied to the image, either on the spatial dimensions, the spectral dimension or both. During the acquisition process, smoothing can come from the point spread

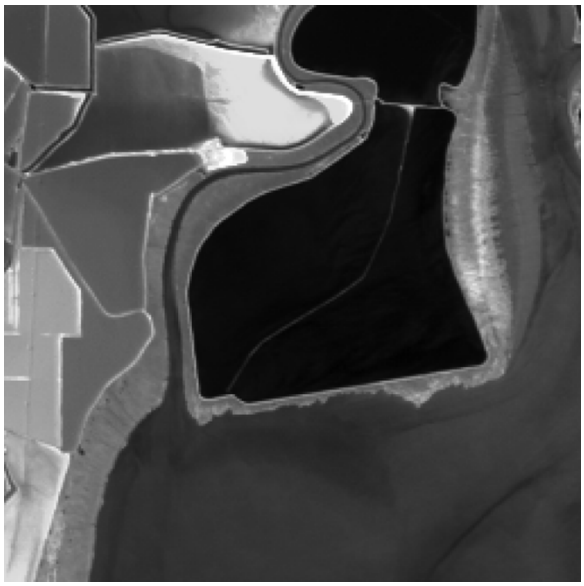

Fig. 4. Moffett2 with uniform zones. Color composition (shown in grayscale) of bands 90 (1211.33 nm), 40 (731.21 nm), and 20 (557.07 nm). This area contains salt evaporators and sea.

Fig. 5. Moffett3 with uneven zones. Color composition (shown in grayscale) of bands 90 (1211.33 nm), 40 (731.21 nm), and 20 (557.07 nm). This area contains man-made targets and vegetation.

function (PSF), from a particular type of compression (wavelets for example tend to blur the image), or from a lower resolution of the sensor. To apply this degradation, a low-pass filter is used. The slope of the filter can be adjusted to change the effect.

The third degradation is a modeling of the Gibbs effect causing ringing around sharp changes. This effect can appear during posttreatments when applying low-pass filters. This effect is simulated using a modified Wiener filter only for the spatial direction.

The last degradation is a JPEG 2000 lossy compression. The verification model (reference implementation of JPEG 2000) version 9.0 was used during these experiments as it implements multiple component transforms. A wavelet transform is first used to decorrelate the spectral bands followed by an application of the JPEG 2000 algorithm with a Lagrangian rate allocation for the subband coefficients.

D. Reference Applications

Many applications for hyperspectral are based on spectral matching. These include target detection and classification. Within the framework of our study, these two types of applications should have been considered. However, in this kind of study, applications must satisfy an implicit requirement, as stated by Ryan [3]. The degradation applied to one image must produce predictable results in the performance of the application for a given level of distortion. As the amount of data is important (about 65 536 pixels to classify for 224 bands), the classification application is on the whole not sensitive to the degradation realization, as every pixel is classified. This requirement would be more difficult to comply with in the case of, say, an anomaly detection. By definition, the number of pixels to be detected by an anomaly detection algorithm is too small to be statistically robust (otherwise they would not be anomaly). Therefore, the application results would strongly depend on the specific realization of the degradation. For example in the case of an additive white noise degradation, if an important degradation happens to be on the anomaly, there is a significant probability that the detection algorithm will fail. For a given level of distortion (e.g., white noise of variance 50), it is not possible to predict the impact on anomaly detection. This is the main reason why the focus in this paper is only on classification applications.

In the case of supervised classification, pixels are classified according to the distance between their spectrum and a spectrum of reference. The reference spectrum can come either from a spectral library containing samples of spectra for different materials, or from a region of interest defined on the image to classify. The measured distance can be defined in different ways. In this paper, a classification based on user-defined region of interest to compute the statistical properties for each class is used. Three different classification processes are studied, namely, *Spectral Angle Mapper (SAM),* using the spectral angle as a distance measure, *mahalanobis classification*, using the mahalanobis distance and a *maximum-likelihood classification* [22]. For each classification, statistics on the regions of interest are calculated: mean spectrum, variance, covariance matrix, etc. Pixels are classified according to their spectral characteristics. In the case of SAM, a threshold is defined. Pixels that are too far from any class remain unclassified. In general, about 6% of pixels will remain unclassified.

Without ground reference to benchmark the performances of the classification (which is not the goal here), only classification variations will be estimated. The score given by the classification will be the percentage of properly classified pixels compared to the reference classification of the original image (Figs. 6 and 7).

E. Evaluation Process

Various degradations have been simulated extensively. For each *situation* (namely one degradation of a certain level applied

Fig. 6. Reference SAM classification for Moffett2, where the black area corresponds to unclassified pixels.

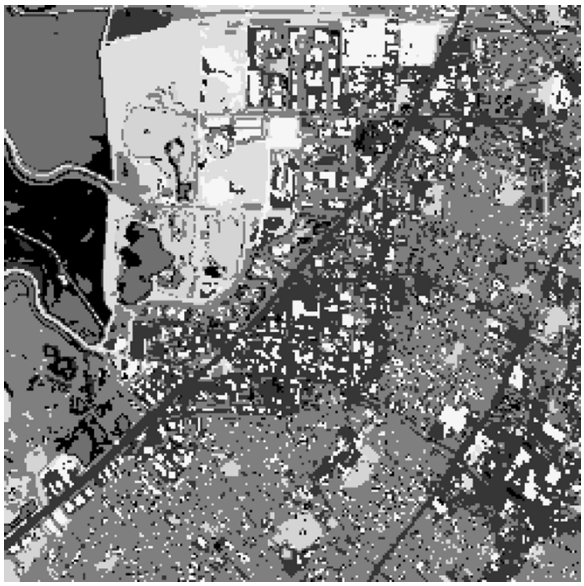

Fig. 7. Reference SAM classification for Moffett3, where the black area corresponds to unclassified pixels.

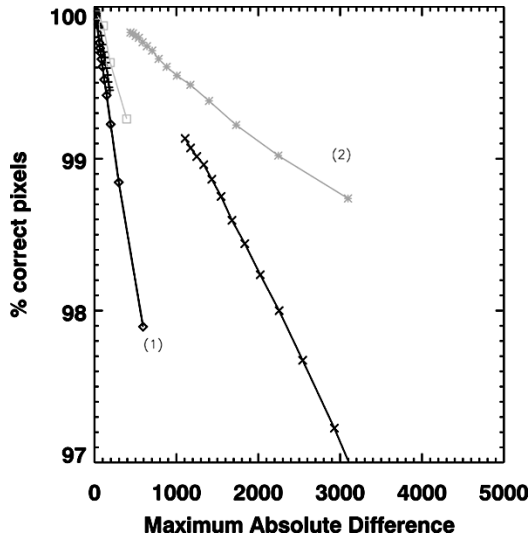

Fig. 8. MAD (5) versus SAM classification. Underestimation of the Gibbs effect (1) and overestimation of the spectral smoothing (2). White noise ($+$), spectral smoothing ($*$), spatial smoothing ($\times$), Gibbs effect ($\diamond$), and JPEG2000 compression ($\square$).

to one image), all quality criteria are calculated and all classification results are measured. To compare these results, a correlation is usually applied. Brill [23] developed a more complete method for the evaluation of quality criteria within the framework of video sequences. However, his method cannot be applied directly to the hyperspectral case due to the difference between human observers and the classification algorithms. While variability is present but small among human observers, classification algorithms are deterministic but can produce very different results depending on the algorithm which is applied.

Therefore, we modify Brill's method. For each situation i corresponding to one degradation of a certain level applied to one image, a score is computed for each quality criterion (O_i, objective score) and for each application (S_i, *subjective* score). For example, the image *moffett2* with an additive white noise of variance 60 is one situation. For this situation, every quality criterion is computed and every application is processed. The curve representing the application performance versus the quality criterion, composed of the points (O_i, S_i), enables us to spot the more sensitive degradations for a given quality criterion.

V. Simulation Results

A. Graphical Interpretation

For each curve (O_i, S_i), the abscissa represents the value of the quality criterion while the ordinate represents the performance of the application. To make the curves easier to read, the value of the quality criterion representing the original quality is on the left side. Likewise, the classification value corresponding to the original quality (100% of correct classification) is on the top.

A quality criterion performs well if the dispersion between curves is low as in Fig. 9. This means that when the amount of error increases for the classification, the quality criterion reacts to it in about the same proportion for every degradation. On the other hand, if the points are scattered, the criterion neglects some degradations and overestimates some others. When the criterion response is concentrated around a vertical direction (Fig. 8 curve 1), the criterion does not react for a degradation that affects the performances. On the other hand, when the response is concentrated around a horizontal direction (Fig. 8 curve 2), the criterion overestimates the impact of the degradation on the application performances, which are almost not affected.

As we can see in Fig. 9, the F_λ criterion (spectral fidelity) seems to give a good estimation of the impact of all degradations on SAM classification. However, as different classification methods have different properties, it is not possible to keep a single criterion for a general estimation.

Two types of criteria can be useful. One type could be criteria that react directly with the application, such as F_λ for

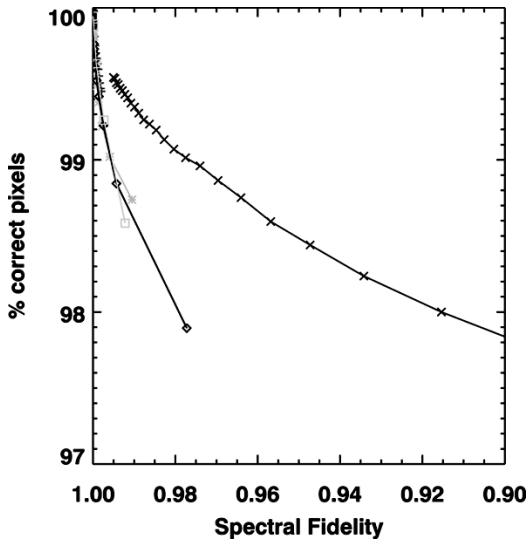

Fig. 9. F_λ (21) versus SAM classification. Dispersion for all degradations is low. The reaction of this criterion is similar with the classification. This criterion gives a reliable estimation of the degradation. White noise ($+$), spectral smoothing ($*$), spatial smoothing ($\times$), Gibbs effect ($\diamond$), and JPEG2000 compression ($\square$).

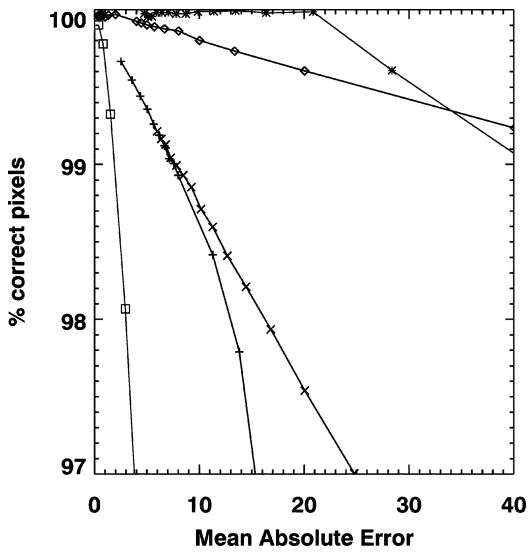

Fig. 10. MAE (7) versus mahalanobis classification. MAE is the criterion most sensitive to the presence of Gibbs effect. White noise ($+$), spectral smoothing ($*$), spatial smoothing ($\times$), Gibbs effect ($\diamond$), and JPEG2000 compression ($\square$).

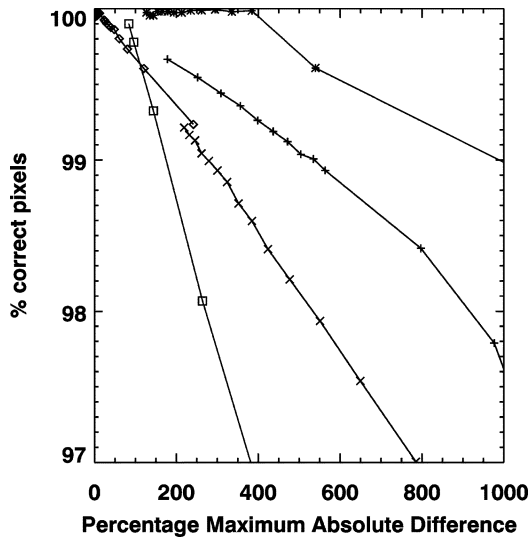

Fig. 11. PMAD (6) versus mahalanobis classification. Appearance of a threshold effect for the spectral smoothing. White noise ($+$), spectral smoothing ($*$), spatial smoothing ($\times$), Gibbs effect ($\diamond$), and JPEG2000 compression ($\square$).

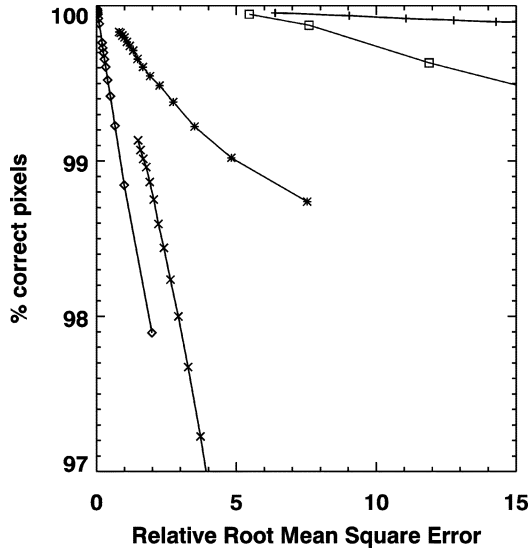

Fig. 12. RRMSE (4) versus SAM classification. RRMSE overreacts to the presence of white noise. White noise ($+$), spectral smoothing ($*$), spatial smoothing ($\times$), Gibbs effect ($\diamond$), and JPEG2000 compression ($\square$).

SAM classification. The other type could be criteria that neglect some degradations and overestimate others. With a panel of well-chosen criteria, it should even be possible to find the nature of the degradation.

While SAM classification is almost insensitive to the presence of white noise in the image (less than 0.5% drop of the percentage of correct classified pixels for a white noise of variance 1000), mahalanobis classification and maximum-likelihood classification are very sensitive to additive white noise (5% drop with a white noise of variance 1000). Another difference appears in the case of spectral smoothing degradation with a threshold effect: for low level of spectral smoothing, classification results are not altered, but above a certain level, the effect is significant. This is due to the influence of class variance for mahalanobis and maximum-likelihood classification. Above a certain level of noise, the two classes become too close and start to merge.

All simulation result curves for all the criteria in all the tested situations can be obtained online.[1] The results obtained vary greatly from one criterion to the other. Some overestimate or underestimate the impact of a set of degradations. Spectral smoothing, for example, is overestimated by most criteria, as in Fig. 10 for MAE criterion. However, two criteria represent its impact well: F_λ and Q_λ (see Fig. 9 for F_λ). In the case of mahalanobis classification, the spectral smoothing causes a threshold effect (Fig. 11). Some criteria such as RRMSE, PMAD, MAE, and MSID are very sensitive to a white noise presence, whereas SAM classification almost does not react to this (Fig. 12).

[1]http://www.enseeiht.fr/~christophe/benchmark

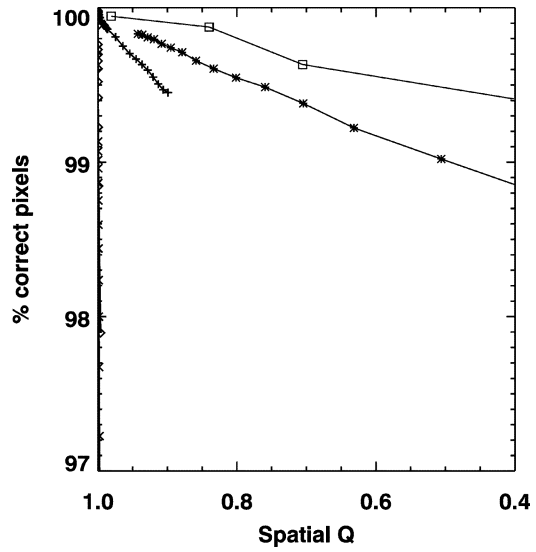

Fig. 13. $Q_{(x,y)}$ (17) versus SAM classification. No sensitivity to the presence of spatial smoothing. White noise ($+$), spectral smoothing ($*$), spatial smoothing ($\times$), Gibbs effect ($\diamond$), and JPEG2000 compression ($\square$).

TABLE II
SENSITIVITY OF QUALITY CRITERIA RELATIVE TO THE DEGRADATIONS (ON MOFFETT2 IMAGE). SELECTED MAXIMUM AND MINIMUM VALUES FOR EACH DEGRADATION ARE REPORTED IN BOLD (SELECTED ACCORDING TO RESULTS ON BOTH IMAGES). WHEN TWO CRITERIA ARE CLOSE TO THE EXTREMUM, ONLY ONE IS CHOSEN TO REDUCE THE TOTAL NUMBER OF CRITERIA

	WhiteN.	Spect.Sm.	Spat.Sm.	GibbsEf.	J2K
MSE	2.94%	21.62%	62.30%	5.40%	7.74%
MAD	1.53%	24.81%	64.60%	2.70%	6.36%
PMAD	23.43%	10.59%	19.20%	1.70%	45.09%
MSS	0.97%	9.69%	81.95%	2.98%	4.41%
RRMSE	**51.54**%	4.39%	8.05%	0.86%	35.16%
MSA	5.38%	9.42%	67.16%	6.74%	11.31%
MSID	17.08%	0.69%	48.85%	1.19%	32.18%
Pearson	0.68%	2.82%	85.58%	0.87%	10.06%
MAE	17.43%	22.30%	29.07%	**14.84**%	16.36%
$Q_{(x,y)}$	2.50%	**35.57**%	**0.24**%	**0.02**%	**61.66**%
Q_λ	0.14%	0.60%	95.80%	1.36%	2.11%
Q_m	2.20%	31.04%	12.74%	0.20%	53.82%
F	2.99%	21.61%	62.18%	5.44%	7.78%
F_λ	**0.20**%	**0.61**%	**96.10**%	0.85%	**2.23**%
$F_{(x,y)}$	2.38%	30.57%	21.12%	1.24%	44.69%
SAM cl.	4.24%	11.39%	60.37%	12.03%	11.97%
Mahal.	12.42%	0.41%	19.95%	1.57%	65.66%
Max.Like.	10.73%	0.01%	10.33%	2.76%	76.17%

$Q_{(x,y)}$ is completely insensitive to the degradation affecting spatial planes like Gibbs effect or spatial smoothing, even if these degradations have an impact on spectra (Fig. 13).

B. Quantitative Evaluation

The graphical representation of the results given in the previous paragraph enables us to infer some trends about the different proposed criteria. However, this is not sufficient. Some quantitative comparisons are necessary. But we are faced with two major difficulties.

First, all criteria results are not directly comparable: their dynamic ranges are completely different. Normalization cannot be considered due to the arbitrary choice of the reference level required.

Second, the sensitivity of one criterion to one degradation is only defined relative to the other degradations. For example, RRMSE is said to be oversensitive to spectral smoothing only because it is relatively less sensitive to other degradations (see Fig. 12). To overcome these difficulties, the relative contribution of each degradation to the criteria is computed.

For each quality criterion, a range of degradation levels is set. This range represents *plausible* degradation levels. For example, the considered values for white noise are variance from 10 to 100 or, for JPEG 2000, compression rate from 3 to 100. The aim is to find out which criterion is the most sensitive to each degradation.

Then, for each criterion C, mean values of the criterion are computed for each degradation. Thus, each criterion is characterized by $\overline{C}_{\mathrm{WN}}$, $\overline{C}_{\mathrm{Spect.S}}$, $\overline{C}_{\mathrm{Spat.S}}$, $\overline{C}_{\mathrm{Gibbs}}$, and $\overline{C}_{\mathrm{JPEG2000}}$, where the notation $\overline{\cdot}$ denotes the mean value and the subscript indicates the kind of degradation. In order to find out which criterion is the most sensitive to each degradation, the above mean values are replaced with their relative contribution, i.e., $\overline{C}_{\mathrm{WN}}/\overline{C}, \overline{C}_{\mathrm{Spect.S}}/\overline{C}, \ldots$ where $\overline{C} = \overline{C}_{\mathrm{WN}} + \overline{C}_{\mathrm{Spect.S}} + \ldots$. This contribution is computed for all criteria and for the performances of the different classification methods. These results are given in the comparative Table II.

The reported values mean that, for example, the contribution to RRMSE is 51.54% from white noise, 4.39% from spectral smoothing, 8.05% from spatial smoothing, 0.86% from Gibbs effect, and 35.16% from JPEG 2000 (the total being 100%). These values depend on the arbitrary choice of distortion ranges and therefore need to be compared with other criteria as well as the applications results. For RRMSE, the comparison with SAM classification values shows that RRMSE overestimates the impact of white noise (51.54% versus 4.24% for SAM classification) and underestimates Gibbs effect (0.86% versus 12.03% for SAM classification), confirming the interpretation of Fig. 12. The presented results are calculated based on the *moffett2* image but the values are very similar to those computed using the *moffett3* image. Extrema in Table II are selected according to the results on both images.

C. Which Quality Criteria?

Graphical interpretation and quantitative evaluation of Table II, presented in the two previous parts, allow us to infer some properties about the different criteria proposed. Among the 15 criteria studied, the most sensitive to additional white noise is the RRMSE, while the most sensitive to Gibbs effect is MAE. Both spatial quality $Q_{(x,y)}$ and spectral fidelity F_λ give very interesting results. The first one, $Q_{(x,y)}$, is the most sensitive to spectral smoothing and JPEG2000 effect while it is the least sensitive to spatial smoothing and Gibbs effect. The second, F_λ, is the most sensitive to spatial smoothing while it is the least sensitive to additional white noise, spectral smoothing and JPEG2000 effect.

These properties are summarized in Table III. Thus, these four criteria, namely, RRMSE, MAE, $Q_{(x,y)}$, F_λ, can be computed on each hyperspectral image to give an accurate estimation of

TABLE III
SENSITIVITY OF FINAL QUALITY CRITERIA

	+ sensitive	- sensitive
White Noise	RRMSE	F_λ
Spectral Smooth.	$Q_{(x,y)}$	F_λ
Spatial Smooth.	F_λ	$Q_{(x,y)}$
Gibbs effect	MAE	$Q_{(x,y)}$
JPEG 2000	$Q_{(x,y)}$	F_λ

the nature of the degradation and of their intensity. To enforce the set of criteria, MAD is added because it gives an upper bound for the error on every digital value of the image cube. The results presented above (graphical curves and quantitative evaluation) were obtained using the *moffett2* image. However, the same conclusions hold for the *moffett3* image, which has different characteristics.

Further, these criteria can be used to qualify the nature of the degradation due the difference in their properties. For example, when combining the RRMSE and the $Q_{(x,y)}$, should the RRMSE indicate a strong degradation and the $Q_{(x,y)}$ not react, it can be concluded that the degradation is probably similar to a white noise. By combining the five defined criteria, more precise estimations can be obtained.

These results, which are first obtained by interpreting the curves presented in Section V-A, are confirmed by the proposed quantitative evaluation of Section V-B.

VI. PERSPECTIVES

Among the 15 quality criteria studied, five of them have been singled out for their properties. As seen above, the five chosen criteria can be used to characterize the nature and the level of the degradation affecting an image and to predict the performance of a given application. However, only classification applications have been tested here; other applications could be added to the evaluation, using the same procedure.

The purpose of this study is to find suitable quality criteria relevant to the impact of several degradations on different hyperspectral classification applications. This paper presents a general method to compare the sensitivity of several mathematical criteria to different hyperspectral image degradations when classification algorithms are applied. This method can be used for testing other criteria, other degradations, and/or other applications.

Moreover, this study shows the relevance of using a set of criteria rather than just one of them. Each criterion has a different sensitivity to different image degradations. Therefore, using a set of criteria, for which the sensitivity to different degradations is known, could reveal a lot of information. Since this criteria set could help to characterize the nature of the degradation affecting an image, it would be also useful during the instrument conception and definition. By simulating the instrument effect on hyperspectral data and using the defined criteria, it would be possible to define the key characteristics of the system to ensure a wide range of applications.

ACKNOWLEDGMENT

The authors wish to thank the National Aeronautics and Space Administration Jet Propulsion Laboratory for providing the hyperspectral images used during the experiments.

REFERENCES

[1] B. Aiazzi, L. Alparone, S. Baronti, C. Lastri, F. Lotti, A. Bertoli, E. Magli, G. Olmo, and B. Penna, "ACHYDA rinal report," IFAC-CNR and Carlo Gavazzi Space and Politenico of Turin, Turin, Italy, Tech. Rep. ACH-RP-IFAC-002, May 2004.

[2] R. E. Roger and J. F. Arnold, "Reversible image compression bounded by noise," *IEEE Trans. Geosci. Remote Sens.*, vol. 32, no. 1, pp. 19–24, Jan. 1994.

[3] M. J. Ryan and J. F. Arnold, "Lossy compression of hyperspectral data using vector quantization," *Remote Sens. Environ.*, vol. 61, pp. 419–436, 1997.

[4] B. Hu, S.-E. Qian, D. Haboudane, J. R. Miller, A. B. Hollinger, N. Tremblay, and E. Pattey, "Retrieval of crop chlorophyll content and leaf area index from decompressed hyperspectral data: The effects of data compression," *Remote Sens. Environ.*, vol. 92, pp. 139–152, 2004.

[5] S.-E. Qian, "Hyperspectral data compression using a fast vector quantization algorithm," *IEEE Trans. Geosci. Remote Sens.*, vol. 42, no. 8, pp. 1791–1798, Aug. 2004.

[6] D. Landgrebe, "Hyperspectral image data analysis," *IEEE Signal Process. Mag.*, vol. 19, no. 1, pp. 17–28, Jan. 2002.

[7] G. F. Hughes, "On the mean accuracy of statistical pattern recognizers," *IEEE Trans. Inf. Theory*, vol. IT-14, no. 1, Jan. 1968.

[8] J. Pearlman, C. Segal, L. Liao, S. Carman, M. Folkman, B. Browne, L. Ong, and S. Ungar, "Development and operations of the EO-1 Hyperion imaging spectrometer," TRW Space and Electronics Group, El Segundo, CA, Tech. Rep., Aug. 2000.

[9] R. E. Simmons and B. V. Brower, "Data characterization for hyperspectral image compression," in *Proc. SPIE Conf. Multispectral Imaging for Terrestrial Application II*, vol. 3119, 1997, pp. 172–183.

[10] R. O. Green, J. E. Conel, J. Margolis, C. Chovit, and J. Faust, "In-flight calibration and validation of the Airborne Visible/Infrared Imaging Spectrometer (AVIRIS)," presented at the *6th Annu. JPL Airborne Earth Science Workshop*, Pasadena, CA, 1996.

[11] L. B. Liao, P. J. Jarecke, D. A. Gleichauf, and T. R. Hedman, "Performance characterization of the Hyperion imaging spectrometer instrument," in *Proc. SPIE Conf. Earth Observing Syst. V*, vol. 4135, W. L. Barnes, Ed., Nov. 2000, pp. 264–275.

[12] European Space Agency, "SPECTRA—Surface Processes and Ecosystem Changes Through Response Analysis," in *The Five Candidate Earth Explorer Core Missions*. Noordwijk, The Netherlands: ESA, 2001.

[13] J. F. Bolton, "Full spectral imaging: a revisited approach to remote sensing," in *Proc. SPIE Conf. Sensors, Systems, and Next-Generation Satellites VII*, vol. 5234, Sep. 2003, pp. 243–251.

[14] M. Carnec, P. L. Callet, and D. Barba, "Full reference and reduced reference metrics for image quality assessment," *Proc. IEEE Conf. Signal Processing and Its Applications*, vol. 1, pp. 477–480, Jul. 2003.

[15] A. M. Eskicioglu and P. S. Fisher, "Image quality measures and their performance," *IEEE Trans. Commun.*, vol. 43, no. 12, pp. 2959–2965, Dec. 1995.

[16] VPEQ, "Final report from the Video Quality Experts Group on the validation of objective models of video quality assessment, Phase II," VQEG, Boulder, CO, and Hillsboro, OR, Tech. Rep., Aug. 2003.

[17] S. Rupert, M. Sharp, J. Sweet, and E. Cincotta, "Noise constrained hyperspectral data compression," in *Proc. IGARSS*, vol. 1, Jul. 2001, pp. 94–96.

[18] B. Aiazzi, L. Alparone, S. Baronti, C. Lastri, L. Santurri, and M. Selva, "Spectral distortion evaluation in lossy compression of hyperspectral imagery," in *Proc. IGARSS*, vol. 3, Jul. 2003, pp. 1817–1819.

[19] G. Motta, F. Rizzo, and J. A. Storer, "Compression of hyperspectral imagery," in *Proc. Data Compression Conf.*, vol. 8, Mar. 2003, pp. 333–342.

[20] Z. Wang and A. C. Bovik, "A universal image quality index," *IEEE Signal Process. Lett.* , vol. 9, no. 3, pp. 81–84, Mar. 2002.

[21] N. Damera-Venkata, T. Kite, W. Geisler, B. Evans, and A. Bovik, "Image quality assessment based on a degradation model," *IEEE Trans. Image Process.*, vol. 9, no. 4, pp. 636–650, Apr. 2000.

[22] J. A. Richards, *Remote Sensing Digital Image Analysis*. Berlin, Germany: Springer-Verlag, 1999.

[23] M. H. Brill, J. Lubin, P. Costa, S. Wolf, and J. Pearson, "Accuracy and cross-calibration of video quality metrics: New methods from ATIS/T1A1," *Signal Process.: Image Commun.*, vol. 19, pp. 101–107, 2004.

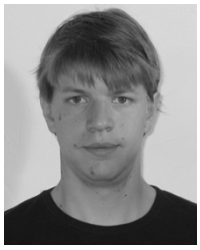

Emmanuel Christophe (S'05) received the Eng. degree in telecommunications from the Ecole Nationale Supérieure des Télécommunications de Bretagne, Brest, France, and the DEA degree from the University of Rennes 1, Rennes, France, in telecommunications and image processing with honors, both in 2003. He is currently pursuing the Ph.D. degree in hyperspectral image compression and image quality, in cooperation with Centre National d'Etudes Spatiales (CNES), Toulouse, France, Office National d'Etudes et de Recherches Aérospatiales (ONERA), Toulouse, Alcatel Space, Paris, France.

In 2003, he worked six months for the National University of Singapore on video compression. His research interests include image and video compression, quality assessment, as well as technologies for remote sensing.

Dominique Léger received the diploma in engineering from the Ecole Supérieure d'Optique, Orsay, France, and the Dr.Ing. degree in 1973 and 1976, respectively.

He has been working as a Research Engineer at the Office National d'Études et de Recherches Aérospatiales (ONERA), Toulouse, France, since 1977. He has been involved in the field of the image quality assessment of Earth observation satellites, particularly in the measurement of defocusing and modulation transfer function of satellite cameras, since 1981.

Dr. Léger is a member of the French Optical Society (SFO) and of the European Optical Society (EOS).

Corinne Mailhes (M'87) received the B.Eng. degree in electronics and signal processing and the Ph.D. degree in signal processing from the Ecole Nationale Supérieure d'Electrotechnique, d'Electronique, d'Informatique, d'Hydraulique et des Télécommunications (ENSEEIHT), Toulouse, France, in 1986 and 1990, respectively.

She is currently an Associate Professor in ENSEEIHT. Her interests lie in the fields of spectral analysis, sampling theory, and data compression.